Gravity Waves in a Forest: A Linear Analysis

XUHUI LEE

School of Forestry and Environmental Studies, Yale University, New Haven, Connecticut

(Manuscript received 16 September 1996, in final form 15 April 1997)

ABSTRACT

Wavelike oscillations are a common form of air motion in the forest canopy at night. This paper investigates the canopy wave phenomenon using a two-dimensional inviscid linear wave model taking into account the drag force exerted on the wave wind components by plant elements and the plant–air heat exchange induced by temperature wave oscillations. The model appears to have adequately reproduced the salient features of a wave event in a boreal aspen forest.

The wave dynamics are investigated as functions of parameters of the background states expressed in analytical form. It is shown that canopy waves are generated by wind shear near the treetops and share features of a Kelvin–Helmholtz disturbance. Because it is located close to the inflection point of the mean wind, the ground exerts a strong stabilizing effect on the wave motions, particularly in a sparse forest. The main role of the canopy drag in the wave dynamics is the creation of the inflection point; its damping effect on wave oscillations themselves is limited to disturbances of wavelengths shorter than that of the fastest growing waves. Wavelength, phase speed, and period of the fastest growing waves, those that are most likely to dominate observations, appear insensitive to static stability.

1. Introduction

Recent forest turbulence experiments have demonstrated that wavelike air motions (referred to as canopy waves hereafter) frequently occur within and above the forest canopy at night. Three mechanisms are commonly invoked to explain wave generation in the lower atmosphere: convective penetration, topographic disturbance, and shear instability (Hooke and Jones 1986; Rees and Mobbs 1988). The first two mechanisms are not responsible for canopy waves as the experimental sites were located on flat terrain and observations were made at night when the whole boundary layer, and the air layer near the canopy in particular, was strongly stratified. One may also speculate that canopy waves are waves that have propagated downward from higher altitudes. This scenario is, however, unlikely because canopy waves possess unique features, such as short and monochromatic wave period and low phase speed, that distinguish themselves from waves that originated in the upper boundary layer.

In the framework of linear wave theory, one necessary condition for shear instability to occur in the statically stable air is that the horizontal wave phase speed must be equal to the background mean wind speed at some height where the gradient Richardson number (Ri) is less than 0.25 (Miles 1961; Howard 1961). The drag force exerted on the moving air by plant elements will reduce the mean wind speed considerably within the vegetation, and as a result a large shear will occur near the canopy top. This shear is often large enough to reduce Ri to values smaller than 0.25 and is most likely to trigger wave generation. Examination of a limited number of wave episodes supports this postulation (Lee et al. 1997). Obviously plant elements are equally efficient in damping wave motions and in reducing the mean wind speed through the bluff–body effect, thus leading to the question of which of the two effects (generation of mean wind shear or damping of wave motions) is the more important one in wave dynamics and the question of whether the critical Ri value of 0.25 derived by Miles and Howard for fluid free of drag elements can be adopted as a criterion for study of canopy waves.

Waves in the course of their generation, propagation, and dissipation can extract, transport, and deposit amounts of momentum and energy large enough to be significant to the state of the atmospheric motion over a range of spatial scales. In the lower atmosphere, waves will yield their momentum to the mean flow at the critical level where phase speed matches the background mean wind speed (Bretherton 1969a,b) and can generate a surface drag at least as large as those associated with turbulent motions (Chimonas 1989; Nappo and Chimonas 1992). Turbulence is created and maintained by random wave breaking or through transfer of kinetic energy from the wave motions under strongly stratified

Corresponding author address: Dr. Xuhui Lee, School of Forestry and Environmental Studies, Yale University, New Haven, CT 06511. E-mail: xuhui.lee@yale.edu

conditions that otherwise would not permit turbulence (Finnigan et al. 1984). Observational studies showed that wave-associated heat and mass fluxes over the vegetation may be large in magnitude that defies interpretation (Lee et al. 1996).

It is well established now that under neutral and unstable conditions the exchange of momentum, heat, and masses between vegetation and the air above are dominated by coherent eddy motions. Drawing an analogy between canopy flow and flow in the plane mixing layer, Raupach et al. (1989) postulated that the coherent eddies are a result of an inviscid instability caused by the mean wind shear near the canopy top. They deduced the existence of inclined double rollers that were supported by mapping of spatial two-point correlation statistics (Shaw et al. 1995). By comparing scales of the mean shear to the mixing layer flow, but without actually performing a linear analysis, they arrived at an estimate of the coherent eddy length scale. One may then argue that nighttime canopy waves resemble daytime coherent eddies in the sense that both are generated by the mean wind shear. By virtue of this resemblance and the frequent occurrence of canopy waves, momentum, heat, and mass exchange associated with them may play an important role in the evolution of the nocturnal boundary layer, although the exact mechanism of the exchange is yet to be discovered.

In recent years increasing attention has been paid to nighttime trace gas exchange over forest vegetation. The CO_2 flux, a measure of the ecosystem respiration rate, is comparable in magnitude to the daytime values, but the time or Reynolds averaging procedure often gives unrealistic results. There is a disturbing possibility that a large portion of the CO_2 released by the forest escapes through some unknown route, and past assessment of the forest sink of the atmospheric carbon may have been subject to large uncertainties. Evaluation of flux data is not the focus of this study, but a fundamental understanding of nocturnal canopy flow is a prerequisite for resolving the issue.

In addition to the evolution of the nocturnal boundary layer and the process of trace gas exchange, there are other reasons to investigate the wave phenomenon. Certain fungus spores (e.g., F. *annosus*) are released from the forest floor at night (Schmidt and Wood 1972). Pressure fluctuations at the soil surface associated with wave motions may help the takeoff through a pressure pumping effect (Baldocchi and Meyers 1991). Unlike intermittent sweep events, which favor rapid settling of particulates to the forest floor (Miller et al. 1996), oscillatory motions will reduce the settling velocity of those particulates whose response time is much shorter than the oscillation period (Stout et al. 1995).

The objective of this study is to investigate the canopy wave phenomenon using an inviscid linear wave model. Governing equations of the model and its numerical method are given in section 2. The model takes into account the drag force exerted on the wave wind components by plants and the plant–air heat exchange induced by temperature wave oscillations. Section 3 compares model outputs with the observation of a wave event in a boreal aspen forest. This comparison shows that the model is physically realistic and provides further support for the notion that canopy waves are generated by shear instability. In section 4, model calculations, using analytical profiles of the mean wind speed and temperature as inputs, yield information about wave growth rate, boundary of the unstable mode, and the influence of canopy density on wave properties. The advantage of using analytical profiles, in addition to speeding up the calculations and to overcoming the lack of data of the mean fields, is the freedom of conducting numerical experiments to investigate background parameters influencing the process, something that is difficult to achieve in field studies.

2. Model

a. Governing equations

We consider a two-dimensional wave propagation in the x–z plane. The coordinate is defined such that z is vertical and x is aligned with the azimuthal direction of propagation. As noted by de Baas and Driedonks (1985), results obtained for the two-dimensional system should also be valid for a three-dimensional system according to Squire's theorem (Betchov and Criminale 1967; Drazin and Reid 1981). The mean state represents a stably stratified hydrostatic atmosphere with potential temperature θ, density ρ, and the x component of the horizontal velocity u, all of which are functions of z only. Wave components of the horizontal wind speed $\tilde{u}$, vertical speed $\tilde{w}$, pressure $\tilde{p}$, and potential temperature $\tilde{\theta}$ are governed by a set of linearized equations for inviscid flow under the Boussinesq approximation and the assumption of incompressibility as

$$\frac{\partial \tilde{u}}{\partial t} + u\frac{\partial \tilde{u}}{\partial x} + \tilde{w}\frac{\partial u}{\partial z} = -\frac{1}{\rho}\frac{\partial \tilde{p}}{\partial x} - F_{\tilde{u}}, \tag{1}$$

$$\frac{\partial \tilde{w}}{\partial t} + u\frac{\partial \tilde{w}}{\partial x} = -\frac{1}{\rho}\frac{\partial \tilde{p}}{\partial z} + g\frac{\tilde{\theta}}{\theta} - F_{\tilde{w}}, \tag{2}$$

$$\frac{\partial \tilde{u}}{\partial x} + \frac{\partial \tilde{w}}{\partial z} = 0, \tag{3}$$

$$\frac{\partial \tilde{\theta}}{\partial t} + u\frac{\partial \tilde{\theta}}{\partial x} + \tilde{w}\frac{\partial \theta}{\partial z} = -S_{\tilde{\theta}}, \tag{4}$$

where g is the gravitational acceleration and t denotes time. Terms $F_{\tilde{u}}$ and $F_{\tilde{w}}$ represent drag forces exerted by plant elements on the wave wind components $\tilde{u}$ and $\tilde{w}$, respectively, and are parameterized as

$$F_{\tilde{u}} = C_d A\tilde{u}u,$$

$$F_{\tilde{w}} = C_d A\tilde{w}u,$$

where C_d is a dimensionless drag coefficient and A is a

plant element area density with units of inverse meters. Term $S_{\tilde{\theta}}$ represents heat exchange between plant elements and the air caused by wave temperature fluctuations and is parameterized as

$$S_{\tilde{\theta}} = C_H A \tilde{\theta},$$

where C_H is a wind-dependent heat transfer coefficient. For computational convenience and in the interest of obtaining a nondimensional group from the wave equation (section 4), instead of the conventional parameterization that C_H is made proportional to $u^{1/2}$ (Meyers and Paw U 1987; Finnigan 1985), C_H is related to the mean wind as

$$C_H = C_h u,$$

where C_h is a dimensionless constant. Numerical difference between the two parameterizations is very small for the range of u considered.

We seek a wave solution of the form

$$(\tilde{w}, \tilde{\theta}, \tilde{u}, \tilde{p}) = (\hat{w}, \hat{\theta}, \hat{u}, \hat{p})(z) \exp[i(kx - \sigma t)] \quad (5)$$

(with the understanding that only the real part be taken as the true solution), where k is the horizontal wavenumber and $\sigma\ (=\sigma_r + i\sigma_i)$ is the complex wave angular frequency. Substituting Eq. (5) into Eqs. (1)–(4) yields a set of equations for $(\hat{w}, \hat{\theta}, \hat{u}, \hat{p})$. An elimination of variables from these equations leads to

$$\frac{d^2\hat{w}}{dz^2} + \frac{1}{a}\frac{d}{dz}(C_d A u)\frac{d\hat{w}}{dz} - \left(\frac{N^2k^2}{aa_1} + \frac{ik}{a}\frac{d^2u}{dz^2} + k^2\right)\hat{w} = 0, \quad (6)$$

where N is the Brunt–Väisäla frequency defined as

$$N = \left(g\frac{d\theta}{dz}\Big/\theta\right)^{0.5},$$

and

$$a = ik(u - c) + C_d A u,$$

$$a_1 = ik(u - c) + C_h A u,$$

with $c\ (=\sigma/k)$ being the complex phase speed. In the absence of plant elements, Eq. (6) reduces to the familiar Taylor–Golstein equation (Gossard and Hooke 1975).

In Eq. (6), profiles of u, θ, and A are either provided by observations (section 3) or by a set of analytical expressions (section 4). The solution of $\hat{w}$ is found from a numerical procedure described below. The wave disturbances of temperature, horizontal wind speed, and pressure are then given by

$$\hat{\theta} = -\frac{\hat{w}}{a_1}\frac{d\theta}{dz}, \quad (7)$$

$$\hat{u} = -\frac{1}{ik}\frac{d\hat{w}}{dz}, \quad (8)$$

$$\hat{p} = \frac{\rho}{ik}\left(\frac{a}{ik}\frac{d\hat{w}}{dz} - \hat{w}\frac{du}{dz}\right). \quad (9)$$

b. Numerical method

The perturbation of the vertical velocity satisfies the condition at the lower boundary,

$$\hat{w} = 0 \quad \text{at} \quad z = 0. \quad (10)$$

At the upper boundary $z \to \infty$, both N and u are assumed to be invariant with height, and therefore $\hat{w}$ satisfies

$$\frac{d\hat{w}}{dz} = ik_z\hat{w} \quad (11)$$

(Lalas and Einaudi 1976; de Baas and Driedonks 1985). Here k_z is the vertical wavenumber and is related to N and u as

$$k_z = \pm\left[\frac{N^2}{(c - u)^2} - k^2\right]^{1/2}. \quad (12)$$

The sign is chosen so that the imaginary part of k_z is positive. This ensures that the wave amplitude decreases with height, or in other words, the wave is trapped in the vertical at higher altitudes.

Equations (6), (10), and (11) constitute an eigenvalue problem. For a given k, $\hat{w}$ at $z = 0$ is a complex function of c_r (real part of c) and c_i (imaginary part of c). An iteration routine is developed to find the roots of

$$\hat{w}(c_r, c_i)|_{z=0} = 0.$$

For a given k, initial values of c_r and c_i are assumed and Eq. (6) is integrated, using a fifth-order Runge–Kutta method with adaptable stepsize control, from a reference height, $z = z_r$, beyond which u and N are virtually constant and Eq. (11) holds, to $z = 0$. If $\hat{w}|_{z=0}$ deviates significantly from zero, new values of c_r and c_i are tried. Strategy for the selection of new c_r and c_i values is based on Broyden's method of root finding for nonlinear systems of equations (Press et al. 1992). The process is repeated until the deviation is smaller than a preset convergence criterion. At this step c_r and c_i values are taken as the true eigenvalues and the corresponding $\hat{w}$ as the true eigenfunction of w. Once $\hat{w}$ is found, Eqs. (7)–(9) allow the three other eigenfunctions, $\hat{\theta}$, $\hat{u}$, and $\hat{p}$, to be determined. Wave amplitude (A_b) and phase angle (ϕ_b) are then calculated as

$$A_b = |\hat{b}|, \quad (13)$$

$$\phi_b = \tan^{-1}(\hat{b}_i/\hat{b}_r), \quad (14)$$

where $\hat{b}_r$ and $\hat{b}_i$ are the real and imaginary parts of $\hat{b}$, which can be any one of $\hat{w}$, $\hat{u}$, $\hat{\theta}$, or $\hat{p}$.

In the following, computations have been performed with $C_d = 0.15$ and $C_h = 0.10$ unless stated otherwise. The C_d value is a typical one for use in canopy flow models (Meyers and Paw U 1986; Lee et al. 1994), and the C_h value is based on the leaf boundary layer resistance formulation of Campbell (1977) and accounts for the effect of turbulence, leaf dimension, and the effect of linearizing the C_H–u relation. Only the results of un-

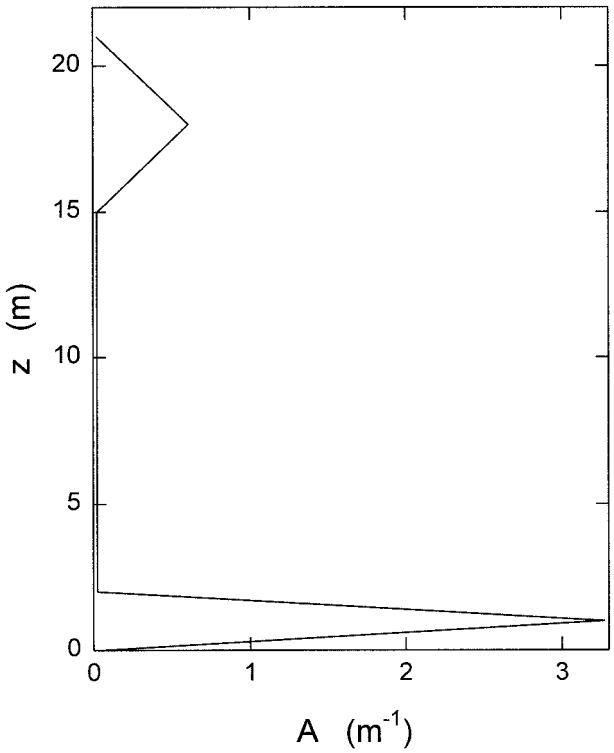

FIG. 1. Plant area density distribution in the boreal aspen forest.

stable modes (c_i or σ_i positive) will be presented since they are the modes that can grow into waves.

3. Results for an observed mean flow

a. Site and data

Details of the site and instrumentation have been documented by Black et al. (1996) and Lee et al. (1997). Only the essential information is reproduced here.

The site (53.7°N, 106.2°W) is located on flat terrain in Saskatchewan, Canada. The forest is an extensive stand of aspen trees about 21 m tall. At the time of observation, the overstory and understory leaf area indices were 1.8 and 3.2, respectively, and are partitioned with height using triangular distributions as shown in Fig. 1.

The platform of turbulence observations was a scaffolding tower 40 m tall. High-frequency (5–20 Hz) time series were provided by three sonic anemometer–thermometers mounted at z = 5.5, 27.7, and 39.1 m and twelve precision fine wire thermocouples at z = 2.2, 4.1, 6.4, 9.5, 12.6, 15.7, 18.8, 21.9, 25.0, 27.7, 31.4, and 39.1 m. These sensors were in operation for most of the BOREAS (Boreal Ecosystem Atmosphere Study) 1994 field campaigns. At a nearby small clearing, a tethersonde carrying a set of wind, temperature, humidity, and ozone sensors was used to probe the air layer at increments of 3 m up to z = 300 m, providing profiles of the mean state needed in model calculations. The tethersonde system was operated mostly in daylight hours, with a few runs made at night. In the following, a 60-min wave event (0239–0339 local time, 4 August), the only event for which tethersonde observation is available, will be used in the model study.

A visual inspection of the temperature time series of this wave event reveals that wavelike motions were clear near the treetops and diminished quickly with distance away from this height, indicating a critical level there (Fig. 2). Clear periodic patterns lasted the full 60-min duration.

Fourier transformation is applied to each of the 10-min segments of the time series and composite spectra and cospectra are formed for the full hour. The spectral analysis yields an estimate of the wave frequency f_w = 0.020 Hz (wave period 50 s). To facilitate the comparison with model outputs, the wave amplitude of the time series b is taken as

$$A_b = (fS_b)^{1/2} \quad \text{at} \quad f = f_w, \tag{15}$$

where f is natural frequency in hertz and S_b is the power spectrum of b. It is found that for a time series with clear periodicity, A_b from Eq. (15) agrees quite well with wave amplitude interpreted visually. Likewise, wave phase angle between b and a reference signal y is estimated as

$$\phi_b = \tan^{-1}(Q_{by}/C_{by}) \quad \text{at} \quad f = f_w, \tag{16}$$

where Q_{by} and C_{by} are the quadrature spectrum and cospectrum between b and y, respectively.

b. Comparison of model results with observations

Figures 3a and 3b show the profiles of vector wind speed, wind direction, and potential temperature obtained from a tethersonde accent during 3:37–3:57 local time. Since the wave model is for a two-dimensional system, an estimate of the azimuthal direction of wave propagation must be made so that the vector wind can be projected along this direction to produce the u profile. This direction has been found from wave-associated wind speed and direction fluctuations (Gossard and Munk 1954; Gossard and Hooke 1975) observed at z = 27.7 m to be 105°, 18° off the mean wind direction at this height. Tenth-order polynomials are then produced by best fitting with a least squares procedure to the observed θ and u profiles and are used in the model calculations.

Figure 3c shows N^2 and Ri profiles based on these polynomials. The value of Ri is below the critical value of 0.25 in the air layer between z = 19 and 36 m. Wind shear at all other heights is not strong enough to trigger instability. (The negative Ri values near the ground and at z = 113 m are an artifact of the polynomial fitting.)

The numerical integration starts at $z_r = 6h$ or 126 m, where h denotes the height of the forest. A range of k values have been tried. Table 1 lists model outputs for three k values to give a sense of the model sensitivity

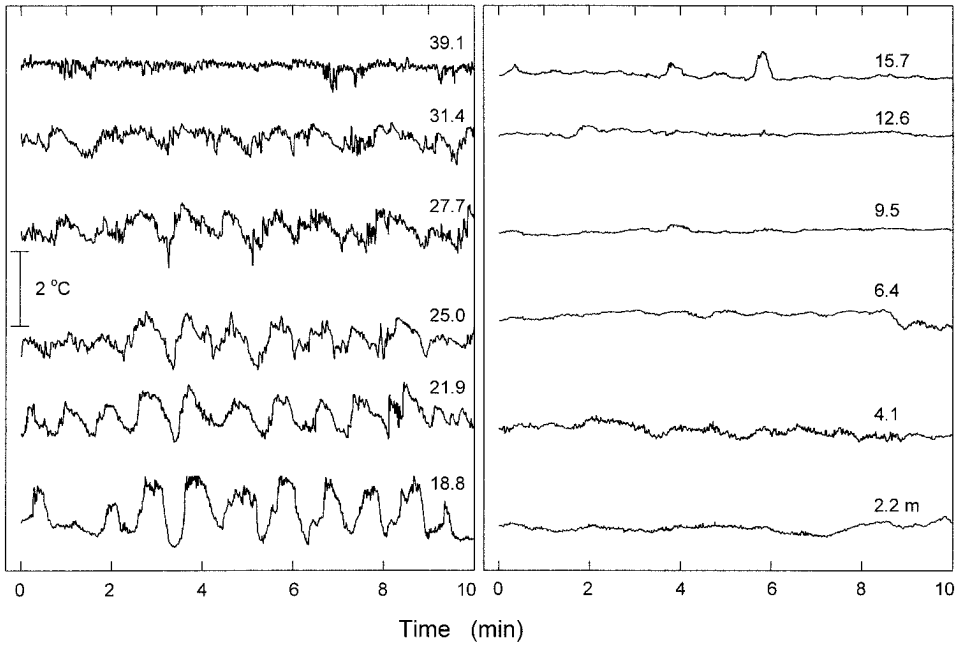

FIG. 2. A 10-min segment of temperature time series in the aspen forest starting at 0239 local time on 4 August.

to *k*. In the following, the solution whose frequency matches the observed one is chosen as the true solution.

The calculated phase speed is believed to be accurate because it matches the mean wind speed near the treetops, thus producing a wave amplitude maximum in accord with observations (Fig. 4). The calculated value also agrees well with the estimate made previously (Lee et al. 1997) with a procedure utilizing the vertical and horizontal wind speed fluctuations (Hooke et al. 1973). The results in Table 1 also indicate that the phase speed estimate is not sensitive to the choice of *k*.

The growth rate is similar to the estimates for waves in the lower boundary layer (de Baas and Driedonks 1985) and is faster than those for waves at higher altitudes (Einaudi and Finnigan 1993). Such growth is not visible during the selected 60-min period but may have occurred prior to that. What is observed is a wave event that had reached some form of quasi-steady state, perhaps because of nonlinear effects, at amplitudes larger than the infinitesimal one to which the linear solution strictly applies (Einaudi and Finnigan 1993). This should be kept in mind when interpreting the model results.

Figure 4 compares the observed and modeled wave amplitudes in the lower 40-m air layer. All eigenfunctions from the linear model, which share a single constant multiplier, have been scaled so that the modeled *w* amplitude matches the observation at $z = 27.7$ m. At $z = 5.5$ and 39.1 m, the modeled *w* amplitude is correct in order of magnitude.

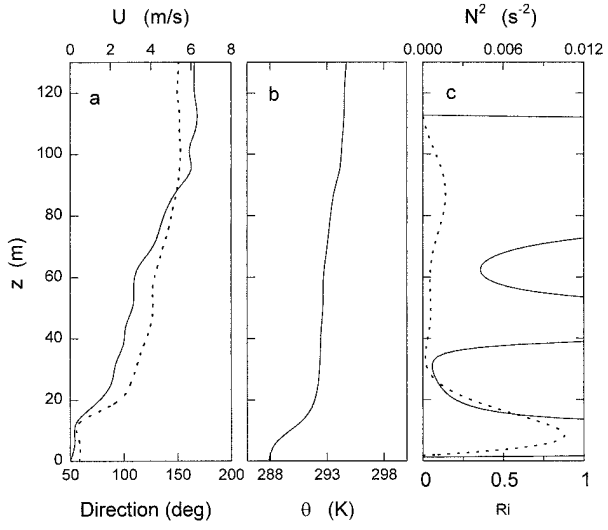

FIG. 3. Tethersonde profiles of (a) vector wind speed (solid line) and direction (dotted line), (b) potential temperature, and (c) the gradient Richardson number for the wind component projected to the azimuthal direction of wave propagation (solid line) and the Brunt–Väisäla frequency squared (dotted line).

TABLE 1. Modeled wave parameters for the wave event at the boreal aspen forest. The observed wave angular frequency is 0.126 rad s^{-1}.

Parameter	Values		
Wavenumber (k, rad m^{-1})	0.102	0.205	0.051
Angular frequency (σ_r, rad s^{-1})	0.126	0.251	0.062
Growth rate (σ_i, s^{-1})	0.0012	0.0008	0.0020
Phase speed (c_r, m s^{-1})	1.23	1.24	1.22
Wavelength (λ, m)	61	31	123

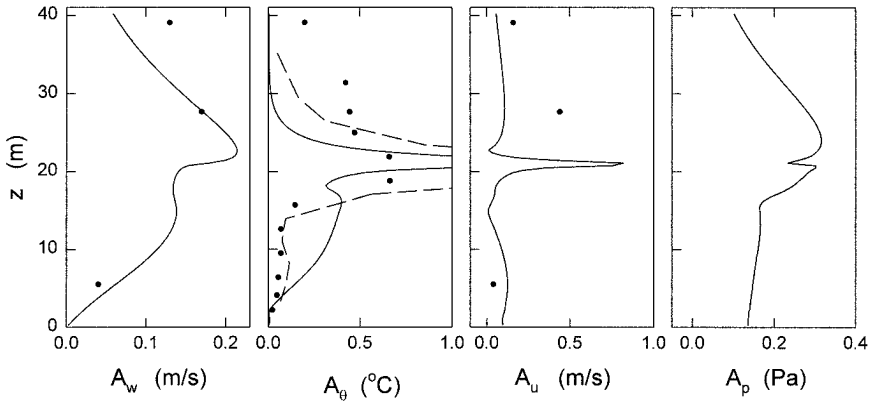

FIG. 4. Comparison of modeled wave amplitudes with observations at the boreal aspen forest: solid line, model output ($k = 0.102$ rad m^{-1}); bullet, observation. The dashed line represents calculations from Eq. (7) by substituting N with observations made on the scaffolding tower.

The agreement for A_θ is not satisfactory, except that the model produces a peak near the treetops that is indicative of a critical level there. The model gives a peak value (2.4°C) two times larger than the observed one. It underestimates A_θ in the air layer above $z = 25$ m and overestimates A_θ below $z = 15$ m. The difference is, however, not an indication of a deficiency in the model itself; rather, it is caused by the fact that the tethersonde temperature profile, which was measured in a clearing of 40 m radius, did not represent accurately the mean state in the forest. The w disturbance is insensitive to the mean θ profile as shown by the sensitivity tests in the next section. This is not the case with the θ disturbance because error in the A_θ calculation is proportional to any error in the θ gradient measurements according to Eqs. (7) and (13). A much better agreement is achieved when N values in Eq. (7) are replaced with observations made on the scaffolding tower (dashed line in Fig. 4).

The model predicts a sharp peak for the longitudinal velocity amplitude, the peak value being 0.8 m s^{-1}. No fast-sampled time series are available for the height of the peak to allow a direct comparison. A slow-response propeller anemometer, located at 2 m above the canopy on a small tower about 150 m away from the scaffolding tower, registered a standard deviation of the horizontal wind speed of 0.25 m s^{-1} for the period of the wave event. After correction for the sensor inertia, the actual wave amplitude might have been comparable to the predicted peak value. It is possible that the predicted peak is real but, as with A_θ, the peak may have been too sharp.

The predicted pressure amplitude peaks at 4 m above the stand and remains essentially constant with height in the trunk space. The amplitude at the soil surface (0.18 Pa) is comparable to the observation by Shaw et al. (1990) in a temperate deciduous forest (median value of 0.20 Pa for 52 half-hourly runs), but is 1–2 orders of magnitude smaller than that associated with wave motions in the upper boundary layer (Egger et al. 1993; Einaudi and Finnigan 1993; Hook et al. 1973; Davis and Peltier 1976). This reinforces the notion that canopy waves and waves in the boundary layer are distinctly different. One alternative interpretation of the surface pressure fluctuations is that they are the vertical integral of the Poisson equation, which expresses the relation between the pressure source term to the fluctuating wind and density fields (Thomas and Bull 1983), and hence the small magnitude is a direct consequence of the characteristic that the air layer undergoing wave perturbations is very shallow.

Figure 5 compares modeled and observed phase angles, both referenced to the vertical velocity at $z = 27.7$ m [cf. Eq. (16)]. A negative phase angle indicates that the signal maximum precedes the w maximum at $z = 27.7$ m. According to the model, the w oscillations should be in phase above the forest and should have a positive phase up to 40° within the stand. This trend appears to reflect the observation in the aspen forest, although previous field studies under mostly convective conditions showed that the w time series were in phase everywhere (Shaw and Zhang 1992). The observed sharp transition in the temperature phase near the treetops, symptomatic of a critical-level phenomenon, is well reproduced by the model. It is noted here that the phase calculation is not prone to the uncertainty in the temperature gradient observation, as it cancels out when the imaginary part is divided by the real part of $\hat{\theta}$ [Eqs. (7) and (14)]. The θ phase within the stand deviates from $\pm 90°$, an angle anticipated for boundary layer waves (de Baas and Driedonks). The agreement for the u phase is poor for reasons that are not clear. The predicted phase for the pressure is negative in reference to w at $z = 27.7$ m, as shown in Fig. 5, or if the local w signal is used as the reference, which agrees in a qualitative sense with Shaw et al. (1990), who reported that, on average, upward fluid motion precedes an increase in pressure at the soil surface in their forest.

It should be pointed out that there are a number of problems with the mean field observation. The most

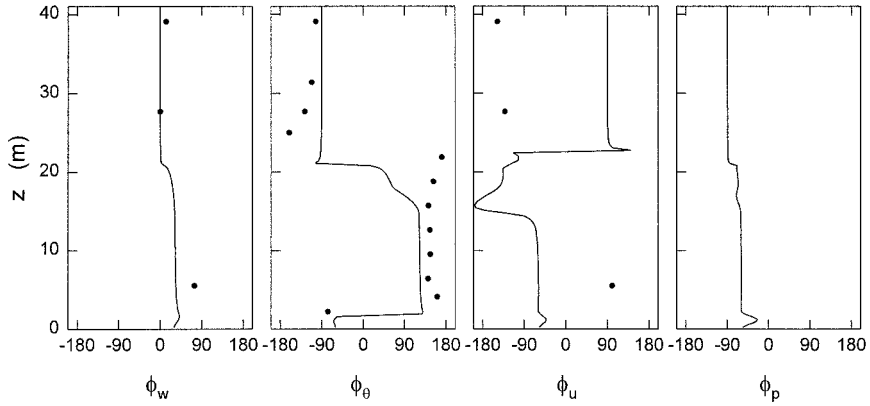

FIG. 5. Same as in Fig. 4 but for phase angle.

serious one is that the tethersonde profiles are a short snapshot of the state of motions rather than the true averages because of the operational procedure. A second source of uncertainties arises from the mismatch in the time of observation: the tethersonde ascent was made when the wave event was almost over, with only a 2-min overlap. A third problem is the spatial separation between tethersonde and tower observations as noted above. Bearing this in mind, it seems fair to conclude that the linear model has reproduced adequately the salient features of the observed wave event. Because of the uncertainties in the mean fields, an assessment of the canopy drag effect on the wave wind and temperature components is not appropriate here. This is best done with the analytical mean profiles.

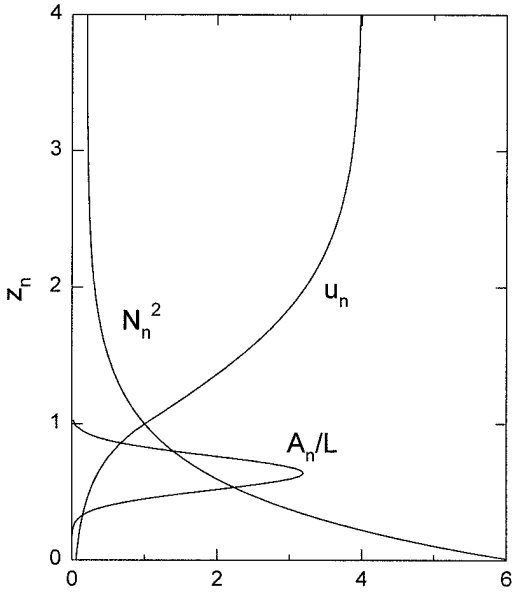

FIG. 6. Analytical profiles of the nondimensional mean wind speed (u_n) and the Brunt–Väisäla frequency (N_n) with parameter values $\alpha_1 = 3.0$, $\alpha_2 = 2.85$ ($L = 4.0$), $\gamma_1 = 0.2$, and $\gamma_2 = 2.0$, and plant element area density divided by plant area index (A_n/L).

4. Results for analytical mean flow

a. Mean fields

In this section, characteristics of canopy waves are investigated as functions of parameters of the background states that are expressed in analytical form (Fig. 6). The nondimensional plant element area density A_n ($= Ah$, h denoting height of the stand) is described by a Gaussian distribution,

$$A_n = \frac{L}{0.125\sqrt{2\pi}} \exp[-(z_n - 0.65)^2/(2 \times 0.125^2)], \tag{17}$$

where $z_n = z/h$, and L is the plant area index noting that $L = \int_0^1 A_n \, dz_n$. The Brunt–Väisäla frequency decreases exponentially with height as

$$N_n^2 = N^2/N_h^2 = (1 - \gamma_1) \exp[-\gamma_2(z_n - 1)] + \gamma_1, \tag{18}$$

where N_h is the Brunt–Väisäla frequency at $z = h$, and γ_1 and γ_2 are parameters to be specified. The N_n^2 value reaches a maximum at the ground surface and approaches a constant of γ_1 at high altitudes to simulate the constant potential temperature gradient above the surface inversion due to radiative cooling (Mahrt et al. 1979).

The mean wind speed follows an exponential function within the stand and a hyperbolic tangent function above, with an inflection point at $z_n = 1$:

$$u_n = \begin{cases} \exp[\alpha_2(z_n - 1)], & z_n \le 1 \\ \alpha_1 \tanh[(\alpha_2/\alpha_1)(z_n - 1)] + 1, & z_n > 1, \end{cases} \tag{19}$$

where $u_n (= u/u_h)$ is the wind speed normalized by that at $z = h (u_h)$. The first derivative of u_n is continuous everywhere, but the second derivative shows discontinuity at $z_n = 1$. As z_n increases, u_n approaches the boundary layer wind equal to $(\alpha_1 + 1)$. Parameter α_2 determines how fast the wind attenuates with depth into the canopy and mainly depends on L. Since one objective

is to investigate how wave features change in response to changes in stand density, a quantitative relationship between α_2 and L is desired. Establishing the relationship involves three steps: simulating the within-stand mean wind profile with a second-order closure model (Wilson and Shaw 1977) for a range of L values, determining α_2 for each L value by fitting the exponential function in Eq. (19) to the model output, and relating α_2 to L by a least squares procedure. The end result is a working formula:

$$\alpha_2 = -0.0296L^2 + 0.6565L + 0.7010. \quad (20)$$

As with the mean profiles, it is convenient to reduce all wave quantities by u_h and h to nondimensional forms, which are denoted by a subscript n (e.g., $k_n = hk$). The nondimensional form of Eq. (6) is

$$\frac{d^2\hat{w}_n}{dz_n^2} + \frac{1}{a_n}\frac{d}{dz_n}(C_d A_n u_n)\frac{d\hat{w}_n}{dz_n} - \left(\frac{N_h^2 h^2}{u_h^2}\frac{N_n^2 k_n^2}{\alpha_n a_{1n}} + \frac{ik_n}{a_n}\frac{d^2u_n}{dz_n^2} + k_n^2\right)\hat{w}_n = 0. \quad (21)$$

The solution of Eq. (21) is now dependent on the nondimensional profiles u_n, A_n, and N_n, as well as a nondimensional group, $r = N_h^2h^2/u_h^2$, which is a stability measure. Since a unique relation exists between r and the more familiar parameter R_m (minimum gradient Richardson number) for a given set of N_n and u_n profiles, it is convenient to discuss the stability dependence of the solution using R_m instead of r.

In the following, all computations except sensitivity tests have been performed with parameter values $\alpha_1 = 3$, $\gamma_1 = 0.2$, and $\gamma_2 = 2$, and three L values, 2, 4, and 6, representing sparse, dense, and very dense stands, respectively. Each L value specifies a u_n profile through the α_2 parameter [Eq. (20)], an A_n profile, and the unique relation between r and R_m. The R_m value is allowed to change from zero corresponding to neutral stability at all heights to an upper limit at which no unstable modes can be found. Integration starts at $z_{rn} = 7$.

b. Results

Figure 7 plots boundary curves that, together with the horizontal axis, bound the regions into which all unstable solutions will fall. The boundaries are determined in the following manner. For each R_m value, eigenvalues of c_r and c_i are calculated for a series of k_n at small increments. The bound of the unstable mode is found by interpolating the two consecutive k_n values at the zero crossing of c_i. In cases when no stable solutions ($c_i < 0$) can be found, the k_n value at which c_{in} is smaller than 0.001 is regarded as the bound of the unstable mode. The uncertainty in the k_n bound estimates from this procedure is no greater than 0.01. As can been seen from Fig. 7, canopy drag effect reduces the critical R_m value from the limit of 0.25 by an amount

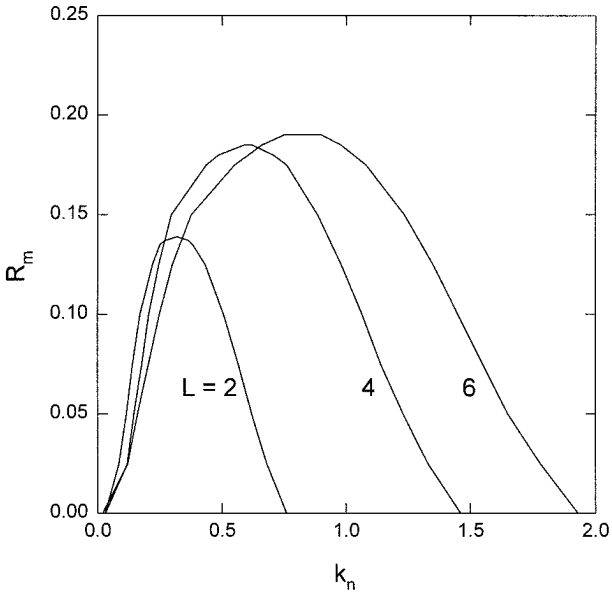

FIG. 7. Boundary of the unstable mode in the wavenumber–static stability plane.

depending on stand density: No unstable solutions can be found with R_m greater than 0.14, 0.19, and 0.20 for $L = 2$, 4, and 6, respectively. The range of k_n over which unstable solutions exist increases with L, and for all simulations the wavenumber is bounded by an upper limit of 2.0. No additional modes have been found, consistent with earlier results by Lalas and Einaudi (1976) and Davis and Peltier (1976), who showed that the presence of the ground very close to the inflection point in the mean wind speed profile, as is the case here, will inhibit secondary modes.

Figure 8 plots phase speed and growth rate as functions of wavenumber for selected static stability conditions. Information about the fastest growing waves (σ_{in} maximum), waves that are most likely to dominate observations, is given in Table 2, where τ_n denotes the reduced wave period and z_{cn} height of the critical level. The growth rate increases rapidly as R_{rn} decreases and as L increases. For a given L, the wavenumber of the fastest growing wave is insensitive to static stability, which once again appears to be symptomatic of the inflection point being close to the ground. A similar behavior is suggested by Lalas and Einaudi's simulations (their Fig. 7). The wavenumber varies from 0.36 for sparse forests to 0.80 for very dense forests (Table 2), corresponding to an actual wavelength range of 17–9h, where h is the height of the stand.

All previous investigations using the linear wave theory have shown unequivocally the property that the wavenumber of the fastest-growing wave is proportional to the inverse of the half-shear-layer depth (Davis and Peltier 1976; Lalas and Einaudi 1976; Raupach et al. 1989; Chimonas and Grant 1984), with the proportionality coefficient falling in the range 0.40–0.46 for

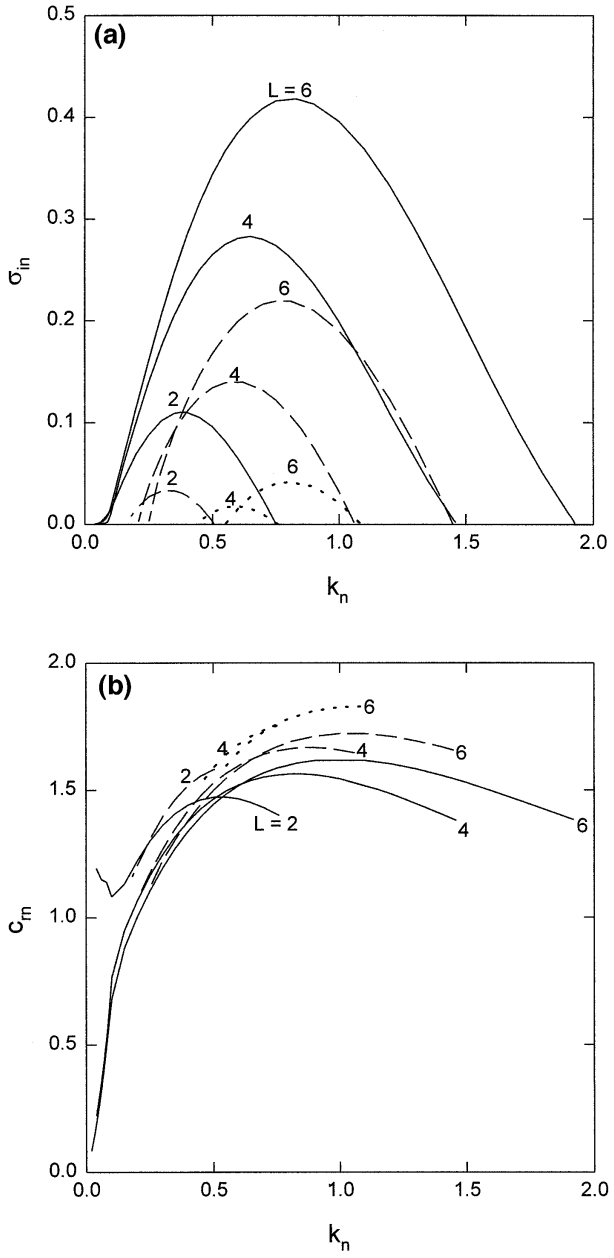

FIG. 8. Growth rate (σ_{in}) and phase speed (c_{rn}) as functions of wavenumber for selected static stability classes and plant area indices (solid line, $R_m = 0$; dashed line, $R_m = 0.1$; dotted line, $R_m = 0.175$). All calculations are made with $\alpha_1 = 3$, $\gamma_1 = 0.2$, and $\gamma_2 = 2$.

$R_m = 0$ or neutrally stratified flow. The proportionality implies that there always exists a size of wave disturbance that is most efficient in smoothing the shear. To apply the finding to canopy flow, Raupach et al. (1989) recommended that the half-shear-layer depth l_n be calculated as the inverse of the wind speed derivative at the inflection point. From this they arrived at an estimate of 0.8 for k_n for canopy flow. Their argument implies the relation $l_n = 1/\alpha_2$ in the present study. It can be shown from data in Table 2 that the resulting product $l_n k_n$ falls in the range 0.13–0.20, which is much smaller than values obtained by other investigators.

TABLE 2. Properties of fastest growing waves calculated with $\alpha_1 = 3$, $\gamma_1 = 0.2$, and $\gamma_2 = 2$ for selected plant area indices and static stability conditions. The half-shear-layer depth (l_n) is given by Eq. (22).

L	α_2	l_n	R_m	k_n	c_{rn}	σ_{in}	z_{cn}	τ_n	$l_n k_n$
2	1.90	1.05	0	0.38	1.43	0.11	1.23	11.6	0.40
			0.1	0.33	1.44	0.03	1.24	13.2	0.32
4	2.85	0.70	0	0.65	1.54	0.28	1.19	6.3	0.46
			0.1	0.59	1.59	0.14	1.21	6.7	0.41
			0.175	0.59	1.67	0.03	1.24	6.4	0.41
6	3.57	0.56	0	0.81	1.60	0.42	1.17	4.8	0.45
			0.1	0.77	1.68	0.22	1.20	4.9	0.43
			0.175	0.81	1.79	0.04	1.23	4.3	0.45

A new method of defining l_n is proposed here that can reconcile the apparent inconsistency. Because wind shear intensities are different within and above the stand, the two air layers must be treated separately. Following the convention (Drazin and Reid 1981), the depth of the shear layer above $z_n = 1$ is α_1/α_2. Similarly, the depth of the shear layer below $z_n = 1$ can be taken as the inverse of the exponent in the wind model ($1/\alpha_2$). The half-shear-layer depth is then given by

$$l_n = \frac{1 + \alpha_1}{2\alpha_2}. \tag{22}$$

This leads to the desired property $l_n k_n = 0.40$–0.46 for $R_m = 0$ (Table 2). Equation (22) suggests that the wavenumber of the fastest growing waves is a function of the shear near the canopy top, as captured in parameter α_2, and the boundary layer wind. Provided that the boundary layer wind is the same, sparser stands favor formation of waves of longer wavelength because the shear layer is thicker. These results indicate that the actual wavelength of canopy waves is a function of a number of parameters including h, L, and α_1 (and is only weakly dependent on static stability). This is at variance with Raupach et al. (1989), who suggested that the wavelength can be scaled by h alone. But they also cautioned that their result should be considered as an order-of-magnitude estimate only.

The mean fields differ from those in earlier numerical studies in two respects: 1) the ground is very close to the inflection point as noted above, and 2) wave motions are subject to the canopy drag effect. Two sets of additional calculations are made for neutral stability ($R_m = 0$) in order to isolate their influence on the wave characteristics. In one case, the ground is hypothetically lowered to $z_n = -10$, thus reducing its effect to a minimum. The resulting wavenumbers of the fastest growing wave remain essentially the same as in Table 2, but the growth rates are faster, with values of 0.32, 0.46, and 0.57 for $L = 2$, 4, and 6, respectively. The relative high percentage of change in the growth rate for the small L value indicates that the ground effect is felt

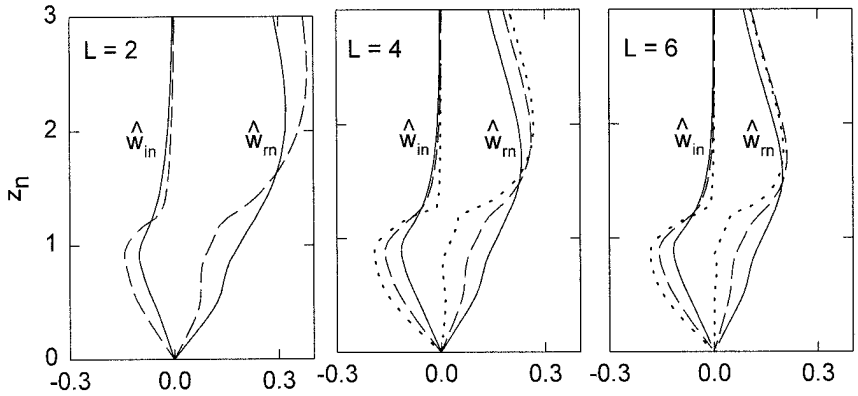

FIG. 9. Real and imaginary part of the w wave disturbance of the fastest growing mode for $R_m = 0$ (solid line), 0.1 (dashed line), and 0.175 (dotted line).

more strongly in a sparse stand. This can be explained by the relationship between the shear layer depth and the stand density: in a sparse stand the shear layer is deep (Table 2) and therefore the ground is located close to the center of the shear layer in a relative sense. It is possible that when L drops below some critical value the ground effect will become so pronounced that no disturbance can grow into waves.

In the second case, the canopy drag effect is removed by setting both drag coefficient C_d and heat transfer coefficient C_h to zero values. The wavenumbers of the fastest growing waves are identical to the values in Table 2. The corresponding growth rates are slightly higher (0.18, 0.37, and 0.52 for $L = 2$, 4, and 6, respectively). The range of k_n of unstable solutions is twice as broad as in Fig. 7, suggesting that the canopy drag is more effective in stabilizing disturbances of wavelengths shorter than that of the fastest growing waves.

To put the values of phase speed in perspective, it is worth noting that shear-generated waves must travel at a speed exactly equal to the mean wind speed at the inflection point in an unbounded shear flow modeled by a perfectly antisymmetric profile (Tatsumi and Gotoh 1960). The equality holds approximately for neutral air when the ground barrier is introduced at a location far away from the inflection point (Lalas and Einaudi 1976; Davis and Peltier 1976). In the present study, phase speed of the fastest growing waves is always greater than unity or the mean wind speed at the inflection point (Table 2) as a result of the asymmetry of the mean field. Calculations for the hypothetical scenario that the ground is lowered to $z_n = -10$ indicate that for current flow configurations phase speed will match roughly the mean wind speed at the center of the whole shear layer, which is located at $z_n = 1.52$, 1.35, and 1.28 for $L = 2$, 4, and 6, respectively. The actual phase speed is reduced from this upper limit by the ground effect and hence the height of the critical level (z_{cn}) will lie below the center of the whole shear layer (Table 2).

The nondimensional wave period (τ_n) shows little variation with the static stability (Table 2). Under neutral conditions, it decreases from 11.6 for $L = 2$ to 4.8 for $L = 6$, emphasizing once again that u_h and h alone are not enough to collapse wave parameters to universal forms. A similar range of variations for coherent eddy motions has been found from a partial survey of observational studies (Raupach et al. 1989). The τ_n values in Table 2 are much higher than that for the wave event in the aspen forest discussed earlier ($\tau_n = 2.9$), a discrepancy presumably caused by the inadequacy of the mean wind profile model [Eq. (19)] in representing the reality for that particular night.

Figure 9 shows the w disturbance of the fastest growing waves. A feature common to all the disturbance profiles is the abrupt shift in phase at $z_n = 1$, the shift being larger in magnitude for more stable conditions. For $L = 4$ the phase angles are 28°, 50°, and 75° for $R_m = 0$, 0.1, and 0.175, respectively at $z_n = 1$, and are about 10° higher at $z_n = 0.1$. Similar magnitudes and patterns exist for $L = 2$ and 6. Additional information concerning the disturbance is given in Table 3, where the vertical wavenumber k_z is defined such that

$$\hat{w} = \exp(ik_z z).$$

The waves are trapped in the vertical or evanescent if the ratio of the real part to the imaginary part of k_z is much smaller than unity and propagating otherwise. As

TABLE 3. Magnitude of the ratio of the real part to the imaginary part of the vertical wavenumber at selected heights for the fastest growing waves.

L	R_m	z_n		
		0.1	1.0	2.0
2	0	0.12	0.30	0.05
	0.1	0.24	0.50	0.02
4	0	0.16	0.36	0.03
	0.1	0.30	0.59	0.01
	0.175	0.44	0.82	0.00
6	0	0.20	0.34	0.02
	0.1	0.34	0.58	0.00
	0.175	0.46	0.80	0.00

TABLE 4. Test of sensitivity of model outputs to the mean fields for $L = 4$, $R_m = 0.1$, and $\gamma_1 = 0.2$.

			Properties of fastest growing waves				
α_1	γ_2	k_n boundary	k_n	c_{rn}	σ_{in}	τ_n	$l_n k_n$
3.0	2.0	0.21–1.06	0.59	1.59	0.14	6.7	0.41
3.6	2.0	0.18–0.84	0.48	1.70	0.11	7.7	0.39
2.4	2.0	0.26–1.36	0.74	1.47	0.17	5.8	0.44
3.0	2.4	0.22–1.05	0.60	1.65	0.14	6.4	0.42
3.0	1.6	0.21–1.06	0.59	1.55	0.15	6.9	0.41

can be seen from Table 3, canopy waves are trapped waves, except in a thin layer close to the canopy top where they appear to be propagating, in accord with the view that the fastest growing waves in a shear layer should be mostly trapped as long as the linear theory holds (Lalas and Einaudi 1976; Rees 1987).

Results of tests of model sensitivity to parameters of the mean field are given in Table 4. In each test, one of the two model parameters (α_1 and γ_2) is changed by 20% from the control. A higher α_1 value, signifying a higher boundary layer wind speed, favors formation of longer waves. A 20% variation in α_1 results in change of a similar proportion in k_n of the fastest growing wave. The product $l_n k_n$, on the other hand, is not sensitive to α_1 variations, supporting the use of Eq. (22) as a measure of the half-shear-layer depth. All wave properties are insensitive to parameter γ_2, which describes the distribution of thermal stratification with height. This appears to be a common feature of shear-generated waves (e.g., Davis and Peltier 1976).

5. Summary and conclusions

The linear model appears to have adequately reproduced the salient features of a wave event in the boreal forest including a slow phase speed, an amplitude maximum and a sharp phase transition of temperature oscillations near the treetops, and a wave pressure fluctuation that appears correct in order of magnitude. Accurate observation of the background state will bring further improvement to the model results.

It is shown that canopy waves are generated by the wind shear near the canopy top. More specifically, they share features of a Kelvin–Helmholtz instability: a phase speed equal to the background wind near the center of the shear layer, a horizontal wavelength proportional to the depth of the shear layer, and an amplitude that decays rapidly away from the region of shear (Davis and Peltier 1976). Some important points from the calculations with the analytical mean profiles are summarized as follows.

1) The critical minimum Richardson number (R_m) is smaller than the theoretical limit of 0.25, the difference depending on stand density (L). An important question is then whether and how frequently R_m remains subcritical in the field. The fact that there exists an air layer of high turbulence or wave intensity a few meters above the treetops [Lee et al. (1996) for a temperate forest; unpublished data from X. Lee et al. for the aspen forest) seems to suggest that the wind shear is often intense enough to generate waves, which in turn break into turbulence, although a definite answer will have to await a detailed examination of the wave climatology.
2) The main role of the canopy drag in the wave dynamics is the creation of an inflection point in the mean wind profile. Its damping effect on wave motions themselves is limited to disturbances of wavelengths shorter than that of the fastest growing wave.
3) The ground exerts a strong stabilizing influence on the wave motions, particularly on those in a sparse stand. It is possible that, when L drops below some critical value, the ground effect will become so pronounced that no disturbance can grow into waves.
4) The wavenumber of the fastest growing wave is proportional to the inverse of the half-shear-layer depth calculated as the average of the shear layer depth within the stand, which is a function of stand density or, more precisely, of the rate of attenuation of the mean wind with depth into the stand, and that above the stand. The value of the proportionality coefficient is between 0.40 and 0.46 for $R_m = 0$, in accord with previous linear analyses of boundary layer waves, and drops slightly as air becomes stably stratified.
5) The wave phase speed is greater than the mean wind speed (u_h) at the top of the stand ($z = h$). The critical level is probably located between $z = h$ and the center of the whole shear layer.

Acknowledgments. Turbulence data were collected in collaboration with Drs. T. A. Black, J. D. Fuentes, G. den Hartog, and H. H. Neumann. Tethersonde data were provided by Dr. R. E. Mickle. The author thanks Dr. R. H. Shaw for providing the computer code of the higher-order canopy flow model and Dr. L. Mahrt for his constructive suggestions. This work was supported in part by National Science Foundation Grant ATM-9629497.

REFERENCES

Baldocchi, D. D., and T. P. Meyers, 1991: Trace gas exchange above the forest floor of a deciduous forest. Part I: Evaporation and CO_2 efflux. *J. Geophys. Res.*, **96** (D), 7271–7285

Betchov, R., and W. O. Criminale, 1967: *Waves in the Atmosphere.* Elsevier, 456 pp.

Black, T. A., and Coauthors, 1996: Annual cycles of water vapor and carbon dioxide fluxes in and above a boreal aspen forest. *Global Change Biol.*, **2,** 219–229.

Bretherton, F. P., 1969a: Waves and turbulence in stably stratified fluids. *Radio Sci.*, **4,** 1279–1287.

——, 1969b: Momentum transport by gravity waves. *Quart. J. Roy. Meteor. Soc.*, **95,** 213–243.

Campbell, G. S. 1977: *An Introduction to Environmental Biophysics.* Springer-Verlag, 159 pp.

Chimonas, G., 1989: Wave drag in the planetary boundary layer over complex terrain. *Bound.-Layer Meteorol.*, **47,** 217–232.

——, and J. R. Grant, 1984: Shear excitation of gravity waves. Part

I: Models of a two-scale atmosphere. *J. Atmos. Sci.,* **41,** 2269–2277.

Davis, P. A., and W. R. Peltier, 1976: Resonant parallel shear instability in the stably stratified planetary boundary layer. *J. Atmos. Sci.,* **33,** 1287–1300.

de Baas, A. F., and A. G. M. Driedonks, 1985: Internal gravity waves in a stably stratified boundary layer. *Bound.-Layer Meteorol.,* **31,** 303–323.

Drazin, P. G., and W. H. Reid, 1981: *Hydrodynamic Stability.* Cambridge University Press, 527 pp.

Egger, J., C. Wamser, and C. Kottmeier, 1993: Internal atmospheric gravity waves near the coast of Antarctica. *Bound.-Layer Meteorol.,* **66,** 1–17.

Einaudi, F., and J. J. Finnigan, 1993: Wave-turbulence dynamics in the stably stratified boundary layer. *J. Atmos. Sci.,* **50,** 1841–1846.

Finnigan, J. J., 1985: Turbulence transport in flexible plant canopies. *The Forest-Atmosphere Interaction,* B. A. Hutchison and B. B. Hicks, Eds., D. Reidel, 443–480.

——, F. Einaudi, and D. Fua, 1984: The interaction between an internal gravity wave and turbulence in the stably-stratified nocturnal boundary layer. *J. Atmos. Sci.,* **41,** 2409–2436.

Gossard, E. E., and W. H. Munk, 1954: On gravity waves in the atmosphere. *J. Meteor.,* **11,** 259–269.

——, and W. H. Hooke, 1975: *Waves in the Atmosphere.* Elsevier Scientific, 456 pp.

Hooke, W. H., and R. M. Jones, 1986: Dissipative waves excited by gravity-wave encounters with the stably stratified planetary boundary layer. *J. Atmos. Sci.,* **43,** 2049–2060.

——, F. F. Hall, and E. E. Gossard, 1973: Observed generation of an atmospheric gravity wave by shear instability in the mean flow of the planetary boundary layer. *Bound.-Layer Meteorol.,* **5,** 29–41.

Howard, L. N., 1961: Note on a paper of John W. Miles. *J. Fluid Mech.,* **10,** 509–512.

Lalas, D. P., and F. Einaudi, 1976: On the characteristics of gravity waves generated by atmospheric shear layers. *J. Atmos. Sci.,* **33,** 1248–1259.

Lee, X., R. H. Shaw, and T. A. Black, 1994: Modeling the effect of mean pressure gradient on the mean flow within forests. *Agric. For. Meteor.,* **68,** 201–212.

——, T. A. Black, G. den Hartog, H. H. Neumann, Z. Nesic, and J. Olejnik, 1996: Carbon dioxide exchange and nocturnal processes over a mixed deciduous forest. *Agric. For. Meteor.,* **81,** 13–29.

——, H. H. Neumann, G. den Hartog, J. D. Fuentes, T. A. Black, R. E. Mickle, P. C. Yang, and P. D. Blanken, 1997: Observation of gravity waves in a boreal forest. *Bound.-Layer Meteorol.,* in press.

Mahrt, L., R. C. Heald, D. H. Lenschow, and B. B. Stanov, 1979: An observational study of the structure of the nocturnal boundary layer. *Bound.-Layer Meteorol.,* **17,** 247–264.

Meyers, T. P., and K. T. Paw U, 1986: Testing of a higher-order closure model for modeling airflow within and above plant canopies. *Bound.-Layer Meteor.,* **37,** 297–311.

——, and ——, 1987: Modeling the plant canopy micrometeorology with higher-order closure principles. *Agric. For. Meteor.,* **41,** 143–163.

Miles, J. W., 1961: On the stability of heterogeneous shear flows. *J. Fluid Mech.,* **10,** 496–508.

Miller, D. R., Y. Wang, K. M., Ducharme, X. Yang, K. Mierzejewski, M. A. McManus, and R. E. Reardon, 1996: Some atmospheric turbulence and stability effects on aerial spray penetration into hardwood forest canopies. *For. Sci.,* **42,** 93–101.

Nappo, C. J., and G. Chimonas, 1992: Wave exchange between the ground surface and a boundary-layer critical level. *J. Atmos. Sci.,* **49,** 1075–1091.

Press, W. H., S. A. Teukoisky, W. T. Vetterling, and B. P. Flannery, 1992: *Numerical Recipes in Fortran.* Cambridge University Press, 963 pp.

Raupach, M. R., J. J. Finnigan, and Y. Brunet, 1989: Coherent eddies in vegetation canopies. *4th Australasian Conf. Heat and Mass Transfer,* Christchurch, New Zealand, University of Canterbury, 75–90.

Rees, J. M., 1987: The propagation of internal gravity waves in the stably stratified atmospheric boundary layer. *Ann. Geophys.,* **5B,** 421–432.

——, and S. D. Mobbs, 1988: Studies of internal gravity waves at Halley Base, Antarctica, using wind observations. *Quart. J. Roy. Meteor. Soc.,* **114,** 939–966.

Schmidt, R. A., and F. A. Wood, 1972: Interpretation of microclimate data in relation to basidiospore release by Fomes annosus. *Phytopathology,* **62,** 319–321.

Shaw, R. H., and X. J. Zhang, 1992: Evidence of pressure-forced turbulent flow in a forest. *Bound.-Layer Meteor.,* **58,** 273–288.

——, K. T. Paw U, X. J. Zhang, W. Gao, G. den Hartog, and H. H. Neumann, 1990: Retrieval of turbulent pressure fluctuations at the ground surface beneath a forest. *Bound.-Layer Meteor.,* **50,** 319–338.

——, Y. Brunet, J. J. Finnigan, and M. R. Raupach, 1995: A wind tunnel study of air flow in waving wheat: two-point velocity statistics. *Bound.-Layer Meteor.,* **76,** 349–376.

Stout, J. E., S. P. Arya, and E. L. Genikhovich, 1995: The effect of nonlinear drag on the motion and settling velocity of heavy particles. *J. Atmos. Sci.,* **52,** 3836–3848.

Tatsumi, T., and K. Gotoh, 1960: The stability of free boundary layers between two uniform streams. *J. Fluid Mech.,* **7,** 433–441.

Thomas, A. S. W., and M. K. Bull, 1983: On the wall-pressure fluctuations in deterministic motions in the turbulent boundary layer. *J. Fluid Mech.,* **128,** 283–322.

Wilson, N. R., and R. H. Shaw, 1977: A higher order closure model for canopy flow. *J. Appl. Meteor.,* **16,** 1197–1205.